MDPI

Article

The Friction of Radially Loaded Hybrid Spindle Bearings under High Speeds

Marcus Gärtner [1,*], Christian Brecher [1], Stephan Neus [1], Hans-Martin Eckel [1], Andreas Bartelt [1], Maik Hoppert [2] and Mohammad Reza Ilkhani [3]

[1] Laboratory for Machine Tools and Production Engineering (WZL) of RWTH Aachen University, Campus-Boulevard 30, 52074 Aachen, Germany; c.brecher@wzl.rwth-aachen.de (C.B.); s.neus@wzl.rwth-aachen.de (S.N.); h.eckel@wzl.rwth-aachen.de (H.-M.E.); a.bartelt@wzl.rwth-aachen.de (A.B.)

[2] MSC.Software GmbH, Hexagon Company, Parkring 3, 85748 Garching, Germany; maik.hoppert@hexagon.com

[3] Power Electronics and Machines Centre (PEMC), Engineering Department, University of Nottingham, Jubilee Campus, Nottingham NG7 2GT, UK; mohammad.ilkhani@nottingham.ac.uk

* Correspondence: m.gaertner@wzl.rwth-aachen.de; Tel.: +49-241-802-4791

Abstract: Friction losses are an important parameter for evaluating the operational behaviour of high-speed rolling bearings. Specifically, in machine tool applications, the bearings are subjected to high radial loads and high speeds, which lead to increased forces in the rolling contact and, as a result, increased bearing friction. In this high-speed application, hybrid spindle bearings, typically made of ceramic balls and steel raceways, show better frictional behaviour compared to full steel-made bearings. Therefore, precise knowledge of the friction characteristics of high-speed hybrid bearings can improve friction models and generalise them to spindle bearings with different types, geometries, and operating conditions. In this article, a new straightforward and cost-efficient method for measuring the frictional torque in spindle bearings is presented. A rigidly arranged 7008 hybrid spindle bearing pair was tested up to rotational speeds of 24,000 rpm and high radial loads of 3 kN. The effects of oil–air and grease lubrication are discussed in characteristic diagrams of the tested bearings. Then, based on the test results, a friction calculation model is presented and validated for the outer race control and minimised power dissipation regarding the influence of radial forces.

Keywords: hybrid spindle bearings; radial load; generator test rig; lubrication; high-speed; machine tool; rigid arrangement; friction calculation

check for updates

1. Introduction

With rising demands on power loss and the associated minimisation of the friction of angular contact ball bearings in tool spindles, precise knowledge of the friction conditions, especially under high speeds and radial load, is essential. As an example based on the friction torque achieved by a proven method and validated on a test rig, a set of bearings that has less power loss in a high-speed application can be selected to reduce the consumed power in the machinery and help reduce the air propulsion. More friction leads to higher temperatures in the rolling contact, which in turn can be measured with a delay by the rising temperature at the bearing's outer ring. Additionally, bearing friction is a reliableindex to compare and validate the performance of the same type of bearings within the size range. In the literature, friction has only been measured for axially loaded bearings over many times [1,2]. As the load distribution on the rolling elements in the axial bearing is almost the same, as an advantage for this type of application, a more differentiated statement about the friction of single balls of the bearing is possible. However, Reference [3] carried out a wide range of friction moment tests for angular contact ball bearings and cylindrical and tapered roller bearings under axial and radial loads on a multiple-bearing test rig, which showed

good agreement with the calculation approaches proposed in [1,4]. In [5], a calculation model for bearing friction was successfully validated using the spindle and tapered roller bearings, but only under axial load and for speeds up to 10,000 rpm. An improved friction model was presented and validated for speed parameters up to 1,600,000 mm/min [6]. However, the radial loads considered with a maximum of 500 N are low for spindle applications. In addition, the hybrid spindle bearings usually used in tool spindles were not considered in this work. For machine tools' application, however, the friction behaviour of radially loaded high-precision bearings for speeds above 10,000 rpm with oil–air lubrication is more of interest. In these cases, the load distribution inside the bearing is non-uniform, and in some cases, a single rolling element can lose contact with the bearing's races. Furthermore, validated friction models can also be used to optimise thermal models for the condition monitoring of spindle tools. A special use case for the validation based on bearing friction is the generator test rig with radial force control in [7]. A multi-pole surface permanent magnet generator that can be used as a source to supply the onboard grid in aircraft has been designed to relieve the load from the bearing. In this application, the radial force control can detect and compensate forces applied to the bearings during operation so that the bearings are relieved and bearing friction is minimised. In this case, due to the system's complexity, measuring the bearings' friction is impossible and having a reliable friction model for the bearings is necessary. Therefore, evaluating the behaviour of each rolling bearing in a separate test rig is necessary by emulating the operational conditions with and without control. In the past, in the standardised test stand concept FE8, the total bearing friction of two or more bearings can be measured for a limited speed range so that frictional torque peaks cannot be directly assigned to each bearing [8]. In the proposed concept, axial and radial forces can be applied to the bearing. Although this concept has been proven for standard applications with low speeds and high loads, e.g., in the field of wind energy or automotive applications, new concepts must be developed to meet the requirements for high-speed applications such as machine tools or aerospace generators. The methodology to measure bearing friction under radial loads and at high speeds presented in this article not only is intended to validate radial force control, but also can be applied to any other high-speed application.

2. Bearing Friction Model

2.1. Calculation of Bearing Friction

Various methods have been developed to calculate the friction in angular contact ball bearings in the past [1,2,5]. In the following, Steinert's approach is presented, which has already been proven successful in previous studies [7]. In this calculation method, the rolling friction due to ball deformation, the raceway ball sliding friction due to rolling motion, and the raceway bore friction in the rolling contact are calculated and then summed up as described in [1,9]. The total bearing frictional torque is then calculated by adding up the friction contributions of the single rolling contacts. Subsequently, the different race control methods and different friction force equilibria are assumed for the outer and inner rings.

2.1.1. Rolling Friction Due to Ball Deformation

In loaded rolling bearings, an elliptical contact surface is formed by the deformation between the rolling element and the raceway. With constant preload and rotation, this flattening of the balls results in an irreversible power loss. The associated frictional torque $M_{roll,B}$ is obtained by integrating the product of the pressure distribution $\Delta p(x,z)$ and the rolling direction x over the rolling contact surface dA from the general Equation (1).

$$M_{roll,B,i} = \int_A \Delta p(x,z) \ x \ dA \tag{1}$$

The deformation of the rolling element during rolling generates heat losses due to the hysteresis effect caused by the material damping. These damping losses occur in the

run-out zone in the rolling contact and can be taken into account in (2) in the form of the damping parameter κ, which is around 0.7% for steel, and the local pressure distribution $\Delta p(x, z)$ [10]. Here, Q stands for the normal force in the rolling contact, a for the length, and b for the height of the semi-axis of the pressure ellipse in the rolling contact.

$$\Delta p(x, z) = \frac{3}{2} \frac{\kappa \, Q}{\pi \, a \, b} \sqrt{1 - \left(\frac{x}{b}\right)^2 - \left(\frac{z}{a}\right)^2} \tag{2}$$

Substituting Equation (2) into (1) and integrating over the length a and width b of the pressure ellipse give the following frictional torque in the rolling contact in (3), which agrees with the result of [11].

$$M_{roll,B,i} = \frac{3}{16} \kappa \, b \, Q \tag{3}$$

The total frictional torque $M_{roll,B}$ referring to the rotation axis of the rolling bearing that is obtained by the summation of the single rolling frictional torques z of the inner i and outer ring o in Equation (4). The speed ratio, consisting of the angular speed of the rolling element ω_b and the outer and inner ring $\omega_{o/i}$, is calculated by neglecting the slip and assuming that the angular speeds of the rolling elements are equal in all rolling bearing contacts.

$$M_{roll,B} = \frac{3}{16} \kappa \left| \frac{\omega_b}{\omega_o - \omega_i} \right| \sum_{k=1}^{z} [(b \, Q)_o + (b \, Q)_i]_k \tag{4}$$

2.1.2. Raceway–Ball Sliding Friction Due to Rolling Motion

Figure 1a depicts the ball raceway contact with the respective coordinate system and velocities. Due to the stress on the ball during operation, a flattened contact ellipse is created in the rolling contact, so that a sliding friction torque is caused between the balls and raceways during rolling (see Figure 1b,c). This results in a velocity profile for the sliding share in the rolling contact, as shown in Figure 1b). During the rolling, the ball spins around its instantaneous centre with the distance c between the axis of rotation and the contact point. Between these two points, the ball slides against the direction of motion, which leads to friction forces in the rolling direction. This effect is reversed in the outer areas of the contact ellipse ($-a < -d$ and $d < a$) (see Figure 1d). Depending on the operational condition, the lubricant, and the surface roughness, the different friction regimes according to the Stribeck curve can occur in the contact area, which is defined by the specific lubricant film height Λ. In the case of very low relative velocities between the contact bodies, solid body friction ($\Lambda = 0$) can be calculated with the Coulomb friction. For medium relative velocities, where the lubricating film has not yet fully formed, there is still occasional solid body friction, and this is referred to as mixed friction. For the range of $0 < \Lambda < 3$, Coulomb friction and elastohydrodynamic (EHD) friction are considered with the weighting factor λ. For high relative velocities in the rolling contact with a specific lubrication height, $\Lambda \geq 3$, a pure EHD friction is assumed, given in Equation (5).

$$\left| \begin{array}{lcc} \text{Solid body friction:} & \Lambda = 0 & F_{slide,R/B} = F_{Coulomb} \\ \text{Mixed friction:} & 0 < \Lambda < 3 & F_{slide,R/B} = \lambda \, F_{Coulomb} + (1 - \lambda) \, F_{EHD} \\ \text{Fluid friction:} & \Lambda \geq 3 & F_{slide,R/B} = F_{EHD} \end{array} \right| \tag{5}$$
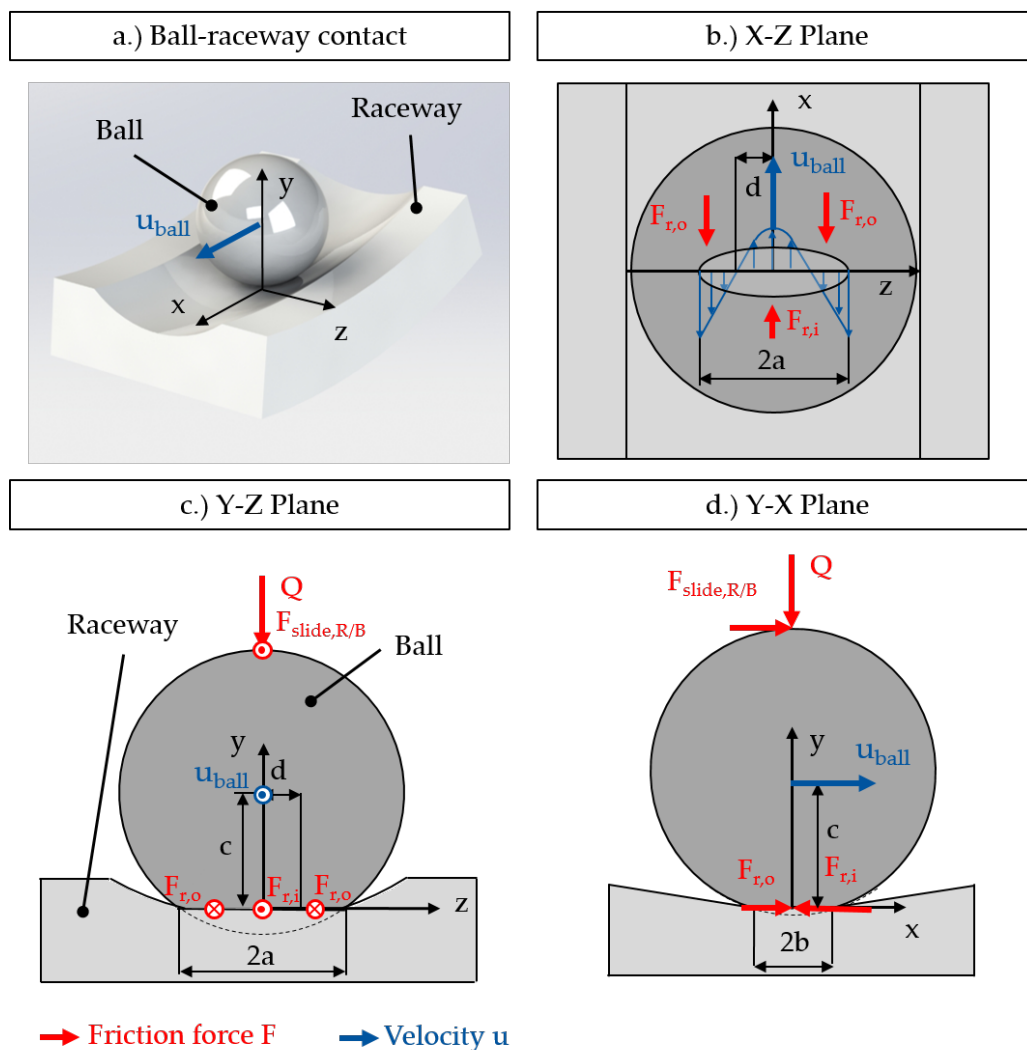
Figure 1. Friction forces and kinematics between the ball and outer raceway according to [1].

The specific lubricant film height Λ depends on the specific lubricant film height h and the effective mean roughness values R_{q1}, R_{q2} and can be calculated with (6).

$$\Lambda = \frac{h}{\sqrt{R_{q1}^2 + R_{q2}^2}} \tag{6}$$

Since the raceways and rolling elements of spindle bearings are usually polished, effective mean roughness values of $R_q = 0.025...0.03$ µm can be assumed [12].

The EHD central lubricant film thickness h independent of temperature is calculated as a function of the dimensionless parameters for speed U, load W, and material G, for the substituted radius R and the reduced thermal reduction factor ϕ_T in (7) [13].

$$h = 4.3 \, \phi_T \, R \, U^{0.68} \, W^{-0.073} \, G^{0.49} \left(1 - e^{-1.28\,\kappa}\right) \tag{7}$$

From the equilibrium of forces on the ball, the Coulomb friction is determined with the inner and outer friction components $F_{r,i/o}$ in Equation (8).

$$F_{Coulomb} = F_{r,i} - F_{r,o} \tag{8}$$

The friction forces can be determined similar to (1) by integrating the pressure distribution in rolling contact considering the coefficient of sliding friction μ_{slide} with (9) and (10).

$$F_{r,i} = 4\,\mu_{slide} \int_0^d \int_0^{x(z)} p_{max} \sqrt{1 - \left(\frac{x}{b}\right)^2 - \left(\frac{z}{a}\right)^2}\,dx\,dz \tag{9}$$

$$F_{r,o} = 4\,\mu_{slide} \int_d^a \int_0^{x(z)} p_{max} \sqrt{1 - \left(\frac{x}{b}\right)^2 - \left(\frac{z}{a}\right)^2}\,dx\,dz \tag{10}$$

The integration limits in the x-direction are the elliptic equation in (11).

$$x(z) = b\sqrt{1 - \left(\frac{z}{a}\right)^2} \tag{11}$$

Substituting Equations (9) and (10) into (8) results in the Coulomb friction force in (12).

$$F_{Coulomb} = \frac{2}{3}\frac{\pi\,\mu_{slide}\,b\,p_{max}}{a^2}(d^3 - 3da^2 + a^3) \tag{12}$$

To determine the distance d between the point where the sliding velocities are zero and the x-axis, a moment equilibrium can be established with Equation (13).

$$\int_{-d}^d l(z)\,dF_r(z) - \int_{-a}^{-d} l(z)\,dF_r(z) - \int_d^a l(z)\,dF_r(z) = 0 \tag{13}$$

The lever arms for the friction moments $l(z)$ are dependent on the variable z and the ball diameter d_B, which is given in (14).

$$l(z) = d_B - \frac{z^2}{d_B} \tag{14}$$

The infinitesimal friction force dF_r is defined as a function of z in (15).

$$dF_r(z) = \mu_{slide}\,p_{max}\sqrt{1 - \left(\frac{x}{b}\right)^2 - \left(\frac{z}{a}\right)^2}dx\,dz \tag{15}$$

The Coulomb friction force can then be found by solving (13) ford and inserting in (12) and simplifying with (16).

$$F_{Coulomb} = \frac{2}{3}\,\mu_{slide}\,\pi\,a\,b\,p_{max} \tag{16}$$

For the determination of the elastohydrodynamic friction coefficient (EHD), a similar approach to Coulomb friction can be used (see Equation (17)), whereby the EHD friction coefficient μ_{EHD} must be determined using Gohar's equations [14,15]. The parameters U, G, and W stand for the EHD parameters and ϕ_T for the thermal reduction factor.

$$F_{EHD} = \mu_{EHD}\,Q = 8.6\,\phi_T\left(\frac{U\,G}{W}\right)^{0.8} Q \tag{17}$$

The total sliding frictional torque between the balls and the raceways in the bearing is calculated by accumulating the contributions of the single rolling contacts considering the rotational speeds ω_B, ω_i and ω_o in (18).

$$M_{slide,R/B} = \left|\frac{\omega_b}{\omega_o - \omega_i}\right|\frac{d_B}{2}\sum_{k=1}^z (F_{slide,R/B,i} + F_{slide,R/B,o})_k \tag{18}$$

2.1.3. Raceway–Ball Bore Friction

During the rolling of the ball on the inner and outer ring, a rotational motion of the ball around the axis of the contact angles of the outer and inner ring occurs, which results in bore friction between the ball and the raceway. This effect always happens at the same time with sliding friction and is taken into account by a separate consideration of the bore velocity. In this case, as well, the friction is calculated similarly to (5) depending on the lubrication condition.

By integrating the stress distribution in the rolling contact multiplied by the distance to the bore axis r and the Coulomb friction coefficient μ, the bore friction is obtained with Equation (19).

$$M_{Coulomb} = F_{Coulomb} r = \mu \int_A p(x,z)\, r\, dA \tag{19}$$

By transforming the local contact stress distribution into polar coordinates the Coulomb friction results in (20).

$$M_{Coulomb} = 4\, \mu\, p_{max} \int_0^{\frac{\pi}{2}} \int_0^{r_\varphi} r^2 \sqrt{1 - \frac{r^2}{r_\varphi}}\, dr\, d\varphi \tag{20}$$

The contact pressure ellipse with the pressure distribution for the derivation of the bore frictional torque is illustrated schematically in Figure 2.
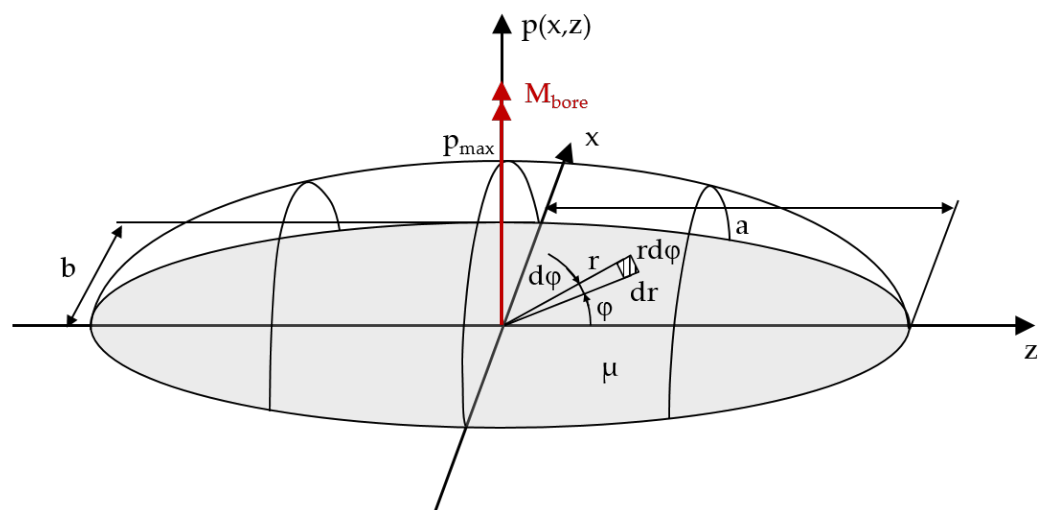

Figure 2. Contact ellipse with pressure distribution for deriving the bore frictional torque.

The auxiliary radius r_φ is determined by the semi-axes a and b and the angle φ in Equation (21).

$$r_\varphi = \frac{b}{1 - \sin^2(\varphi) \cdot \left(1 + \left(\frac{a}{b}\right)^2\right)} \tag{21}$$

By a subsequent integration of Equation (20) by the angle $\pi/2$ and the radius r, one obtains the friction moment in Equation (22).

$$M_{Coulomb} = \frac{1}{4}\, \pi\, \mu\, p_{max}^3\, b^3 \int_0^{\pi/2} \frac{d\varphi}{\sqrt{(1 - (k_0 \sin(\varphi)^2)^3}} \tag{22}$$

The variable k_0 is calculated by the semi-axes a and b of the contact ellipse in (23).

$$k_0 = \sqrt{1 - \left(\frac{b}{a}\right)^2} \tag{23}$$

The solution of the integral is given in [16], and the coefficient of friction can be solved by Grekoussis' equations [17]. The final equation for determining the Coulomb bore moment between the ball and the raceway is then given in (24).

$$M_{Coulomb} = \frac{1}{8} \, \pi^2 \, \mu \, p_{max} \, (b \, \mu_{Hertz})^2 \tag{24}$$

The EHD moment for the fluid friction share can be calculated by the following integral in (25).

$$M_{EHD} = 4 \, \frac{\omega_B}{h} \int_0^b \int_0^{z(x)} \eta(\theta, p) \, (x^2 + z^2) dz dx \tag{25}$$

The integral limit in the z-direction results again from the ellipsoid Equation (26).

$$z(x) = a \, \sqrt{1 - \left(\frac{x}{b}\right)^2} \tag{26}$$

If the lubrication condition is known, the bore torque can be determined for the single rolling contact and for the total bearing with the corresponding transmission ratios of the angular velocities in (27).

$$M_{bore,R/B} = \sum_{k=1}^{z} \left[\left| \frac{\omega_{B,o}}{\omega_o - \omega_i} \right| M_o + \left| \frac{\omega_{B,i}}{\omega_o - \omega_i} \right| M_i \right]_k \tag{27}$$

2.1.4. Total Bearing Friction Torque

According to Steinert's approach, the friction types irreversible deformation work $M_{roll,R/B}$, the sliding friction $M_{slide,R/B}$, and the bore friction $M_{bore,R/B}$ between the bearing rings and balls are determined separately. The single shares are summarised according to Equation (28) as follows [1]. Since an oil–air lubrication is used in the tests with a rather small lubrication amount of 150 µL/h, splashing losses are neglected in this approach.

$$M_{tot} = M_{roll,R/B} + M_{slide,R/B} + M_{bore,R/B} \tag{28}$$

For a more precise understanding of the effective elements of the friction cage, friction should also be taken into account in future investigations, which in some cases show a major influence, which was addressed by the work of [18,19]. However, there is still a lack of sufficient understanding of the ball motion in the cage under radial load to consider it in the superimposed approach presented in this work.

2.1.5. High-Speed Ball Motion

To calculate the friction in angular contact ball bearings, force equilibria between the ball and raceway were assumed, which are briefly explained below. For high-speed applications, an outer race control is usually used based on a force equilibrium on the outer ring including external, centrifugal, and frictional forces (see the left part of Figure 3). In this case, a bore motion occurs only at the inner ring. Hong gave a comprehensive overview of this race control theory [20]. This approach is also suitable for a first approximation calculation under axial loads. However, in order to achieve higher accuracy, especially under radial load, other methods must be used. In another approach, proposed by [21], the frictional losses at the outer ring and on the inner ring are minimised, which is also depicted in Figure 3 on the right side. A similar approach was used by Gupta [22]. Furthermore, there is the inner race control theory, which is common for low-speed applications and which is, therefore, neglected for the following discussions of the experimental results in Section 5.1.
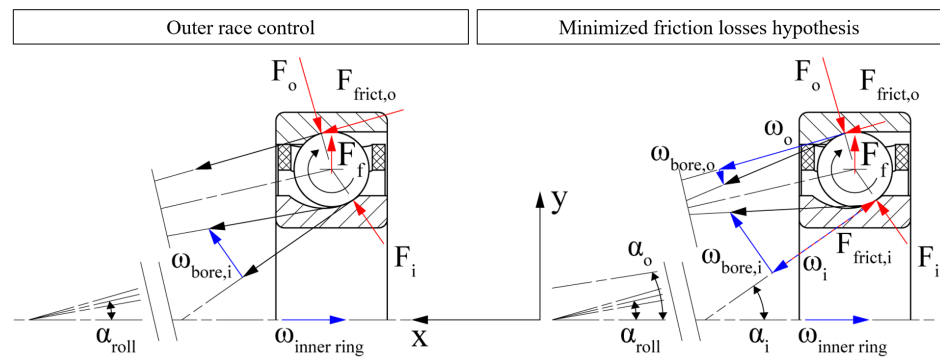
Figure 3. Outer race control and minimised friction loss hypothesis according to [21].

3. Experimental Methods

A modular test rig concept was presented in [23], specially developed for the testing of high-speed rolling bearings of different types and sizes by slight adaptions of the shaft and the housing. A radial load unit to measure the bearing friction of the test bearings with the test bearing was attached to the shaft of the modular test rig. This test setup including the bearings, lubricants, and test program, is described in the following.

3.1. Bearings and Lubricants

In the tests, a rigidly arranged hybrid spindle bearing pair of size 7008 was used, which was also part of the generator test rig described in [7]. The test bearing data are given in Figure 4. The precision class of the bearing was P4; the balls were made of silicon nitride; the raceways were made of bearing steel 100Cr6. The bearings were ground by the manufacturer to a defined preload of 65 N, and due to a shaft interference of the load unit of about 5 μm, an axial preload force of 150 N per bearing was established in the bearing package.
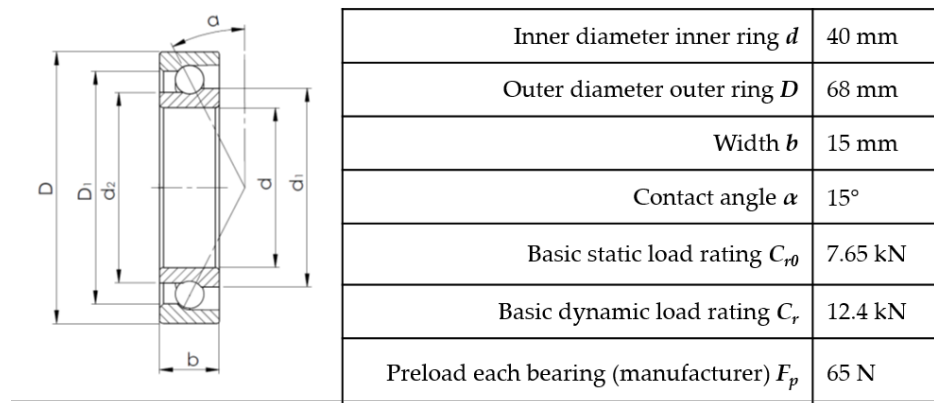

Inner diameter inner ring d	40 mm
Outer diameter outer ring D	68 mm
Width b	15 mm
Contact angle α	15°
Basic static load rating C_{r0}	7.65 kN
Basic dynamic load rating C_r	12.4 kN
Preload each bearing (manufacturer) F_p	65 N

Figure 4. Test bearing data of spindle bearing type SKF 7008/HCP4AH1DGA [24].

A purely filtered spindle bearing oil of the viscosity class ISO VG 68 was used, the properties of which are listed in Table 1. This lubricant is used in high-speed applications such as machine tools and is characterised by its high-speed parameter nxD_m of 2.5 10^3 m/min. For the test with grease lubrication, high-speed grease was selected. The grease, which is based on a synthetic hydrocarbon ester oil, is commonly used in spindle bearings and also has a high-speed parameter nxD_m of 2 10^3 m/min (see Table 1). The grease contains additives for corrosion protection and polyurea thickener. The oil is injected at a diameter of 51.6 mm according to the manufacturer's recommendation [24].

Table 1. Lubricants.

Lubricant	Unit	Oil	Grease
Name	-	Klübersynth FB-4 68 [25]	Klüberspeed BF 72 − 22 [26]
Oil	-	polyalphaolefin	synthetic hydrocarbon ester oil
Thickener	-	-	polyurea
Additives	-	-	corrosion protection
Oil separation	-	-	≤3
Density ρ ($20°$)	(g/cm^3)	0.86	0.92
Kin. viscosity ν ($40°$)	(mm/s^2)	68	22
Speed parameter nxD_m	(10^3 m/min)	2.5	2

3.2. Test Setup

The test setup with the cross-sectional view of the radial load unit, its front view, and the position of the friction force sensor are depicted in Figure 5. The load unit was attached to the test shaft of a high-speed rolling bearing test rig. The test rig and load unit were driven by a synchronous motor with a maximum speed of 30,000 rpm and a power of 15 kW. The outer rings of the test bearings were axially clamped by two housing plates and were rotatable and supported by a needle bearing. The housing plates were connected to a force transducer of HBK type SM2 to measure the bearing friction by an elastic tube. Since the expected friction forces were relatively low, the sensor had a measuring range from 0 to 20 N. The distance between the rotational axis and the force sensor is given in Figure 5b with 51.5 mm. Radial forces up to 3 kN were applied by a hydraulic cylinder on a stamp fixed to the needle bearing. On the stamp, a strain-gauge-based force sensor was attached to a flexure bearing to measure and control the actual radial force.
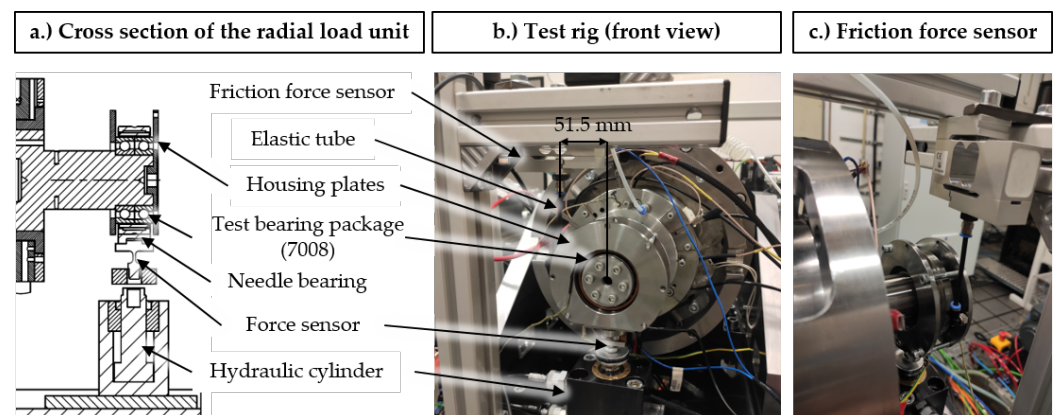
Figure 5. Test setup with the front view and cross-sectional view.

3.3. Test Program

The test program to investigate the bearing friction torque is shown in Figure 6. In a step run from 3000 rpm to 24,000 rpm, the bearing was exposed to varying radial loads. For each speed step, the radial loads were applied after a warm-up phase, starting at 250 N up to 3000 N. The short loading phases of 10 s per load cycle ensured that the internal thermal conditions in the bearing were nearly constant. As soon as the desired radial force was reached in the load step, the bearing friction was measured and the average value over 1 s was calculated. Under oil–air lubrication, tests were carried out with a lubrication quantity of 150 µL/h, and 300 µL/h and for grease lubrication, a series of tests with a grease quantity of 2 g per bearing. Each experiment was repeated a total of three times.
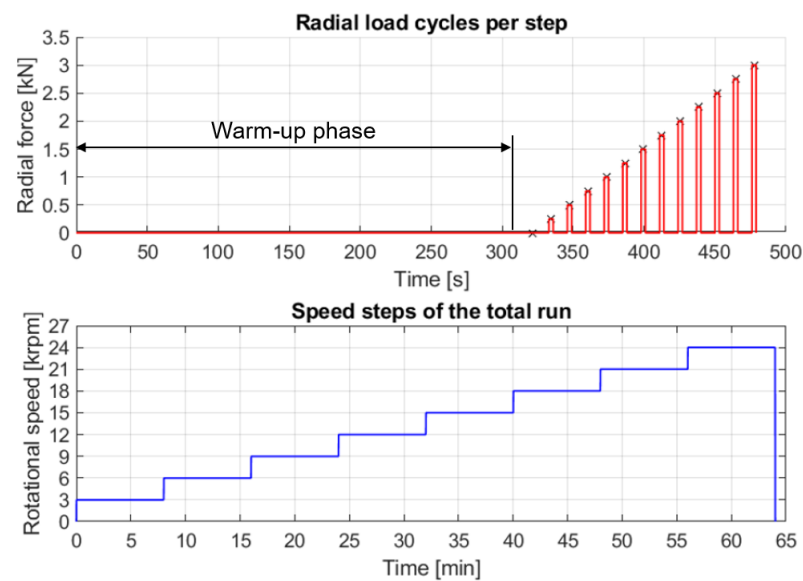
Figure 6. Test program [27].

4. Results

Experimental Results

The test results for different lubrication quantities are shown exemplary in Figure 7 for single tests in characteristic diagrams as a function of radial load and speed. The diagram in the left of Figure 7a shows the frictional torques of the bearing package for an oil lubrication quantity of 150 µL/h. In particular, at 6000 rpm, there was a relatively strong increase in the frictional torque, leading to a friction torque of 0.066 Nm for a radial load of 3 kN. Due to the rising radial load, the load distribution in the bearing changed, so that single balls experienced a loss of contact. The other balls that remained in the load zone experienced a significantly higher load, which was measured in the increasing frictional torque. As the speed increased, however, this effect decreased sharply. Only above 18,000 rpm, the frictional torque increased slightly again. Due to the high speeds, a decent lubricant film build-up can be assumed at this speed. Nevertheless, fluid friction losses became bigger with increasing rotational speed, and above 6000 rpm, the influence of the radial load decreased with higher rotational speeds. A possible reason for the increased frictional torque at speeds up to 9000 rpm could be increased splashing losses for this operation point since there was no oil suction system, which is in line with the findings in [28]. At higher speeds, the oil was carried out of the bearing by rotation, so that losses due to an excessive amount of oil were minimised.
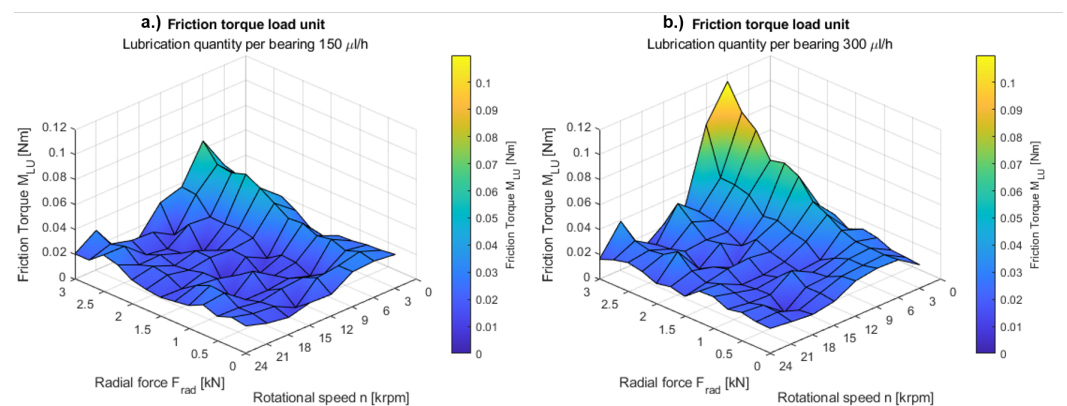

Figure 7. Bearing friction as a function of speed and radial load for different lubrication quantities [27].

If the lubrication quantity was increased to 300 µL/h, this effect was reinforced, as shown in the characteristic diagram in Figure 7b, and the friction of the bearing package increased. Especially at the operating point at 6000 rpm and 3 kN radial load, the friction torque almost doubled with 0.11 Nm. This behaviour can be attributed to the doubled lubrication quantity, which led to increased fluid friction. In general, the qualitative trend for an increased lubrication quantity could be reproduced in several test repetitions. Similar behaviour can be observed in the comparison between oil–air and grease lubrication shown in Figure 8. Figure 8a also shows a test with a lubrication quantity of 150 µL/h, and Figure 8b illustrates the results of a test with a grease-lubricated bearing pair. The bearing was operated with grease lifetime lubrication, which means that a grease quantity of 2 g was added to the bearing once. After a grease distribution run, the base oil precipitated from the grease, which lubricated the rolling contact with the minimum necessary quantity [29]. Again, at 6000 rpm, a strong influence of the radial load could be observed, i.e., an increasing radial load resulted in a strong increase of the friction torque. At a radial load of 3 kN, a frictional torque of 0.0765 Nm was achieved for 6000 rpm. The repeatability of this phenomenon of the friction torque peak at 6000 rpm, regardless of lubrication, indicated that it may be also related to the experimental setup. Based on this result, another possible reason for this behaviour could be a resonance phenomenon leading to strong vibrations of the load unit, which resulted in increased friction values.
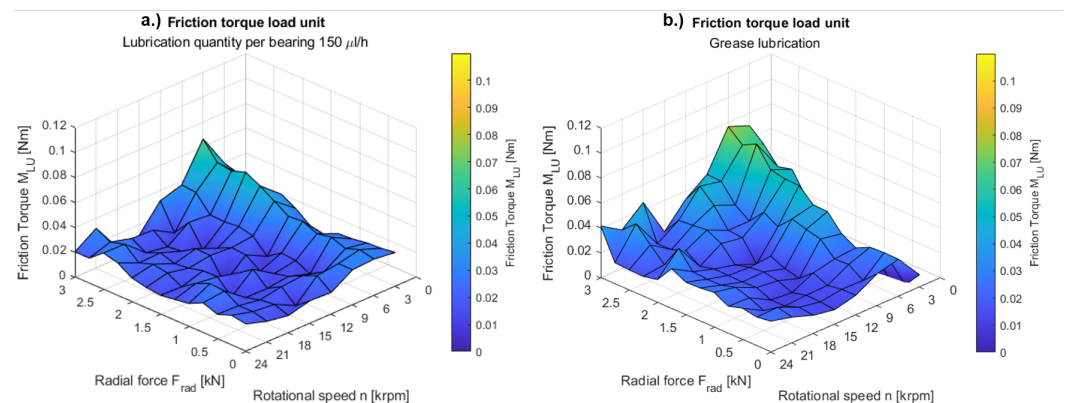
Figure 8. Bearing friction with oil and grease lubrication [27].

With rising speed, the friction then decreased again, similar to oil–air lubrication. However, due to a slightly more uneven distribution of the grease in the bearing, there were increasingly more friction torque peaks at high loads and speeds (see Figure 8b). Nevertheless, the comparison between the results of oil–air and grease lubrication also showed good qualitative repeatability.

The deviations of the measurements over the speed steps and radial loads with their mean values are exemplarily illustrated for oil–air lubrication with 300 µL/h in Figure 9. For pure axial load and a low radial load up to 1 kN, the measurements showed good repeatability. In the case of higher radial loads, especially for 3 kN, higher deviations occurred. One possible reason for this behaviour may be that due to, at high loads, just a few balls were in contact, leading to a strongly discontinuous operational behaviour of the spindle bearing package. This effect was reinforced at the friction peak for 6000 rpm, where an unstable friction behaviour could be observed. In general, it can be seen that the friction measurement of angular contact ball bearings with low preload and high radial forces became difficult due to the increasing loss of contact between the ball and the raceway.
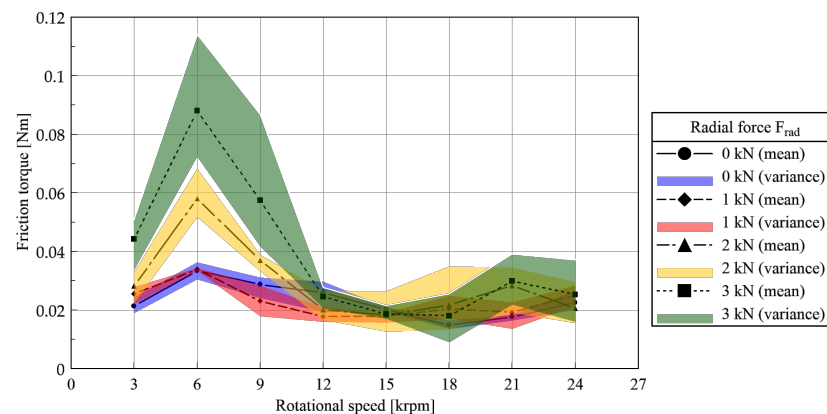
Figure 9. Deviations of the measurements over the speed steps and radial loads for a lubrication quantity of 300 µL/h.

5. Discussion

5.1. Validation of the Calculation

To validate the calculation methodology presented in Section 2.1, a simplified shaft–bearing system was set up in the simulation software MTPlus [23,30]. This Matlab-based software is a combination of an earlier spindle calculation program NewSpiLad [31] and the single bearing calculation program WinLager [32] and is used for research purposes of the WZL. The simulation model with the calculation parameters are given in Figure 10. The focus was on the radial load unit with the investigated spindle bearing package of type 7008, attached to a shaft driven by a motor. The actual osculation of the bearings was measured and considered in the calculation. The hydraulic radial force was applied to the shaft, and the housing of the load units was supported by a fixed floating arrangement. Since the load unit was supported against the piston of the hydraulic cylinder under radial load in the test, this was taken into account in the form of the supports. Due to the fact that the housing tilted only slightly relative to the total length of the shaft, this was simulated by two supports. The floating bearing of the second support was intended to prevent thermal clamping in the simulation.
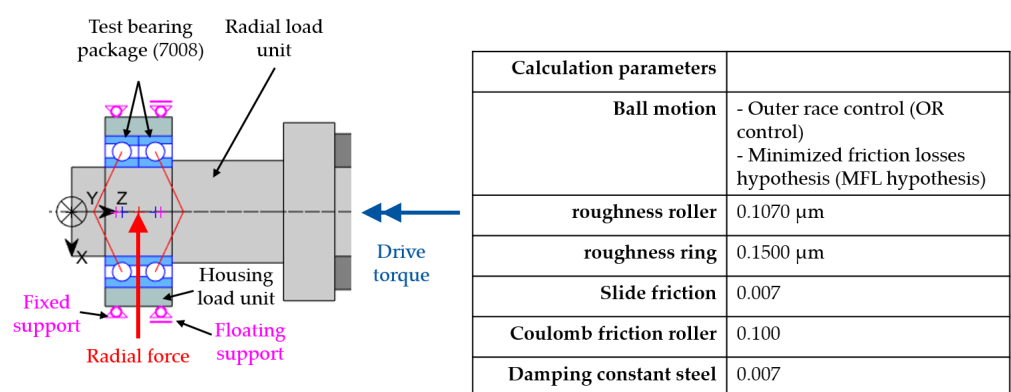

Figure 10. Simplified shaft–bearing model of the load unit in MTPlus with friction values of [1,33].

The average friction torque was calculated according to the approach of [1], presented in Section 2.1, for the ball motion theory of outer race control and the minimised friction hypothesis described in Section 2.1.5 [21]. The comparison between the calculated bearing friction according to the approach of Steinert [1] and the measured spindle bearing friction is given in Figure 11. A linear increase of the shaft temperature was assumed, which was 65° at 24,000 rpm, and the housing temperature was considered to be 60° at this speed.
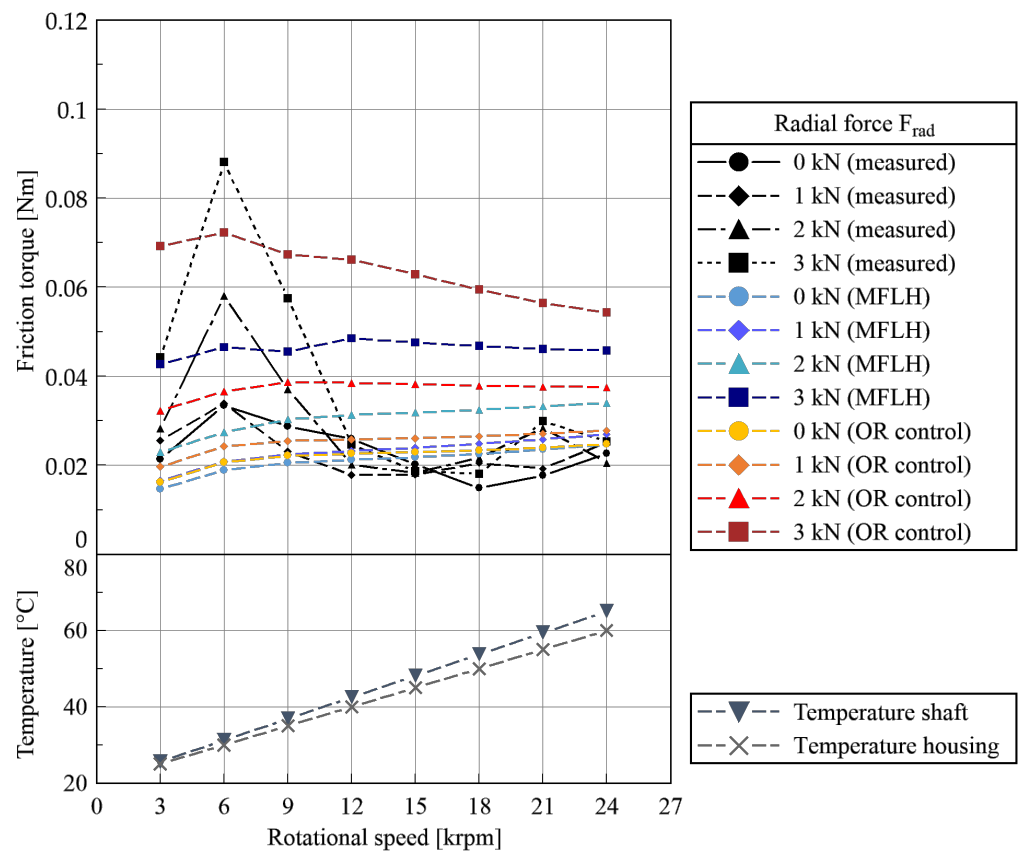
Figure 11. Comparison of measured and calculated friction of the spindle bearing package [27].

In Figure 11, the mean measurement values from Figure 9 are plotted for the tests with lubrication of 300 µL/h for different radial loads and rotational speeds. The calculated values showed good agreement for the MFLH and outer race control from 12,000 rpm and radial loads up to 1 kN. With higher radial loads, there were considerable deviations between the measurement and calculation. In general, the calculations with the MFLH showed lower friction values compared to the outer race control, as expected. Due to the low preload of the package with increasing radial loads, fewer balls were loaded, so the friction losses due to ball deformation rose. This was supported by the additional calculations of the maximum contact surface stresses for the different radial loads, shown in Figure 12.
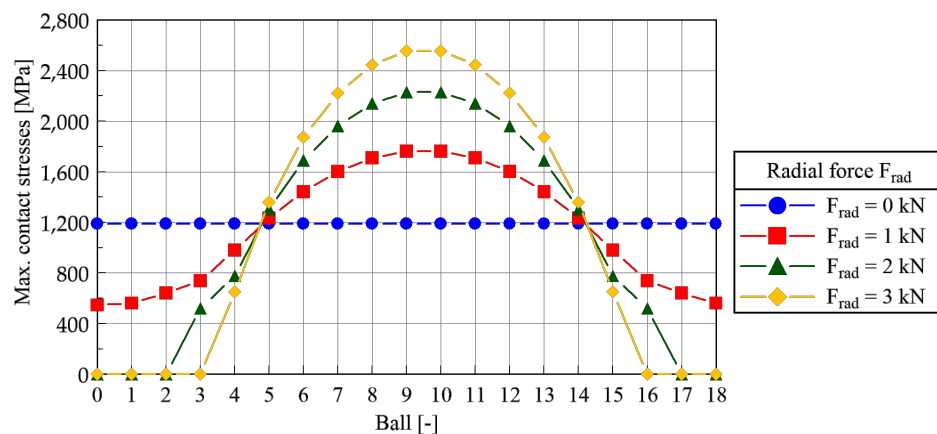

Figure 12. Max. contact stresses at the inner raceway of the bearing for each ball and increasing radial loads [27].

Further possible reasons for the overestimation of the friction torque by calculation can be attributed to considering a high value of sliding and bore friction between the ball and raceway. Although these shares were taken into account by considering sliding and boring velocity separately, nevertheless, the coefficients of friction could be also adjusted. In Figure 13, the calculated single friction shares for a radial load of 3 kN based on the MFLH are shown as dependent on the rotational speed. Boring friction accounted for the largest share of total friction, followed by sliding friction. Due to increasing sliding friction caused by the increasing speed, the boring motion decreased so that the share of boring friction was slightly reduced. Friction due to deformation work was the lowest in comparison and remained almost constant.
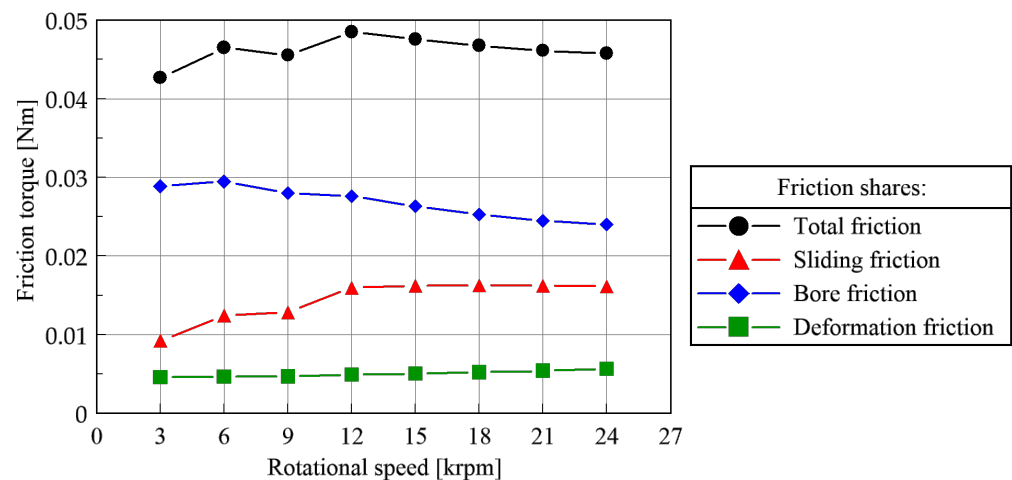

Figure 13. Single friction shares for 3 kN radial load based on the MFLH [27].

Moreover, the friction torque peak at 6000 rpm and increasing radial load were not represented by the calculation. However, these influences were not taken into account in the calculation approach presented here, as the minimum oil quantities introduced into the rolling contact were difficult to quantify in the case of oil–air lubrication. This may be attributed to a better lubricant film formation at high speeds than assumed and, thus, significantly lower friction.

Furthermore according to the calculation for outer race control in 3 kN radial load and rising rotational speed, the friction decreased. This effect can be attributed to an increasing loss of preload caused by excessive radial loads and increasing rotational speeds, leading to increased centrifugal forces and a reduction of the contact surface on the inner ring. Furthermore, the rising temperature difference between the outer and inner rings resulted in a further reduction of the preload force, which reinforced this effect.

6. Conclusions

This paper presented a new straightforward and cost-efficient methodology for measuring bearing friction in radially loaded hybrid spindle bearings. Therefore, a high-speed bearing test rig with an additional radial load unit was designed to measure the frictional torque of hybrid spindle bearings of size 7008. The bearings were investigated under very high rotational speeds up to 24,000 rpm and radial loads up to 3 kN. In several tests, the methodology showed good repeatability, e.g., as well in the comparison of an oil–air and grease-lubricated test. Besides this, it could be illustrated that an increase in the lubrication quantity led to a friction increase under radial loads. The measurements were validated using the approach of Steinert to calculate bearing friction, which showed good agreement for low radial loads up to 1 kN [1]. Nevertheless, the calculation deviated considerably from the measurement at higher radial loads of 3 kN, which can be attributed to a better fluid film formation at higher speeds in the experiment. Due to its easy and cost-efficient

implementation, especially with small bearing sizes, this approach can be used to obtain knowledge about bearing friction under radial loads and to improve simulation models.

Institutional Review Board Statement: Not applicable.

Informed Consent Statement: Not applicable.

Data Availability Statement: Zenodo: The Friction of radially loaded hybrid spindle bearings under high speeds https://zenodo.org/record/7986707 [27]. This project contains the following underlying data (accessed date 14 March 2023):

- Figure 6—Test program.csv;
- Figure 7—Bearing friction as a function of speed and radial load for different lubrication quantities.csv;
- Figure 8–Bearing friction with oil and grease lubrication.csv;
- Figure 9—Deviations of the measurements over the speed steps and radial loads for a lubrication quantity of 300 µL/h.csv;
- Figure 11—Comparison of measured and calculated friction of the spindle bearing package.csv;
- Figure 12—Max. contact stresses at the inner raceway of the bearing for each ball and increasing radial loads.csv;
- Figure 13—Single friction shares for 3 kN radial load based on MFLH.csv.

Conflicts of Interest: The authors declare no conflict of interest.

Abbreviations

The following abbreviations are used in this manuscript:

WZL	Werkzeugmaschinenlabor (Laboratory for Machine Tools and Production Engineering of RWTH Aachen University)
EHD	Elastohydrodynamic
OR	Outer raceway
MFLH	Minimised friction loss hypothesis
MAGLEV	Measurement and analysis of generator bearing loads and efficiency with validation
CS2JU	Clean Sky 2 Joint Undertaking

Nomenclature

In the following, the variables used are described:

A	Area (m^2)
a	Length of the semi-axis of the pressure ellipse in the rolling contact (m)
b	Height of the semi-axis of the pressure ellipse in the rolling contact (m)
d	Distance between the point with no sliding velocities and the x-axis (m)
d_B	Ball diameter (m)
$dF_r(z)$	Infinitesimal friction force (N)
$F_{Coulomb}$	Coulomb friction (N)
F_{EHD}	Elastohydrodynamic friction (N)
$F_{r,i}$	Inner friction component (N)
$F_{r,o}$	Outer friction component (N)
$F_{slide,R/B}$	Sliding friction (N)
G	Dimensionless material parameter (-)
h	Temperature-independent EHD central lubricant film thickness (-)
k_0	Substitute variable (-)
$l(z)$	Lever arms for the friction moments (m)
$M_{bore,R/B}$	Total raceway–ball bore friction torque (Nm)
$M_{Coulomb}$	Coulomb bore friction torque (Nm)
M_{EHD}	EHD torque for the fluid friction share (Nm)
$M_{roll,B}$	Total rolling friction torque (Nm)
$M_{roll,B,i}$	Single rolling friction torque of the inner ring (Nm)
$M_{roll,R/B}$	Total raceway–ball rolling friction torque (Nm)
$M_{slide,R/B}$	Total raceway–ball sliding friction torque (Nm)
M_{tot}	Total bearing friction torque (Nm)
nxD_m	High-speed parameter (m/min)
Q	Normal force in the rolling contact (N)
p_{max}	Maximum pressure (N/m^2)
R	Substituted radius (m)
r	Distance to the bore axis (m)
r_φ	Auxiliary radius (m)
x	Coordinate direction (rolling direction) (m)
U	Dimensionless speed parameter (-)
W	Dimensionless load parameter (-)
z	Coordinate direction (transverse to rolling direction) (m)
$\Delta p(x,z)$	Pressure distribution (N/m^2)
η	Viscosity (Pas)
θ	Temperature (K), (°C)
κ	Damping parameter (-)
Λ	Specific lubricant film height (-)
λ	Weighting factor (-)
μ	Coulomb friction coefficient (-)
μ_{EHD}	Elastohydrodynamic friction coefficient (-)
μ_{Hertz}	Hertzian coefficient of the large pressure surface semi-axis a (-)
μ_{slide}	Sliding friction coefficient (-)
ϕ_T	Thermal reduction factor (-)
φ	Angle in polar coordinates (rad)
ω_b	Angular speed of the rolling element (s^{-1})
$\omega_{B,i}$	Bore angle speed at the inner ring (s^{-1})
$\omega_{B,o}$	Bore angle speed at the outer ring (s^{-1})
ω_i	Angular speed of the inner ring (s^{-1})
ω_o	Angular speed of the outer ring (s^{-1})

References

1. Steinert, T. Das Reibmoment von Kugellagern mit Bordgeführtem Käfig. Ph.D. Thesis, RWTH Aachen, Aachen, Germany, 1996.
2. Rossaint, J. Steigerung der Leistungsfähigkeit von Spindellagern durch Optimierte Lagergeometrien. Ph.D. Thesis, RWTH Aachen, Aachen, Germany, November 2013.
3. Wang, D. Berechnung der Wälzlagerreibung Aufgrund Weiterentwickleter Rheologischer Fluidmodelle. Ph.D. Thesis, Leibniz University Hannover, Hannover, Germany, 2015.
4. Zhou, R.S.; Hoepprich, M.R. Torque of Tapered Roller Bearings. *ASME J. Tribol.* **1991**, *113*, 590–597. [CrossRef]
5. Houpert, L. Ball Bearing and Tapered Roller Bearing Torquem Analytical, Numerical and Experimental Results. *Tribol. Trans.* **2008**, *45*, 345–353. [CrossRef]
6. Tong, V.C.; Hong, S.W. Improved formulation for running torque in angular contact ball bearings. *Int. J. Precis. Eng. Manuf.* **2018**, *19*, 47–56. [CrossRef]
7. Brecher, C.; Neus, S.; Gärtner, M.; Eckel, H.M.; Hoppert, M.; James, B.; Gerada, C.; Degano, M.; Ilkhani, M.R.; Di Nardo, M. *Design of an Aircraft Generator with Radial Force Control*; Open Research Europe: London, UK, 2022.
8. DIN. Mechanisch-Dynamische Prüfung auf dem Wälzlagerschmierstoff-Prüfgerät FE8: Teil 1: Allgemeine Arbeitsgrundlagen, December 2016. Available online: https://www.beuth.de/de/norm/din-51819-1/262168002 (accessed on 14 March 2023).
9. Harris, T.A.; Kotzalas, M.N. *Advanced Concepts of Bearing Technology: Rolling Bearing Analysis*, 5th ed.; CRC Press: Boca Raton, FL, USA, 2007.
10. Hertz, H. Ueber die Berührung fester elastischer Körper. *J. Für Die Reine Angew. Math. (Crelles J.)* **1882**, *91*, 156–171.
11. Tood, M.J.; Johnsons, K.L. A model for coulomb torque hysteresis in ball bearings. *Int. J. Mech. Sci.* **1987**, *29*, 339–354. [CrossRef]
12. Hoischen, H. *Technisches Zeichnen*, 38th ed.; Cornelsen: Essen, Germany, 2022.
13. Chittenden, R.J.; Dowson, D.; Dunn, J.F.; Taylor, C.M.; Johnson, K.L. A theoretical analysis of the isothermal elastohydrodynamic lubrication of concentrated contacts. I. Direction of lubricant entrainment coincident with the major axis of the Hertzian contact ellipse. *Proc. R. Soc. Lond. A Math. Phys. Sci.* **1985**, *397*, 245–269. [CrossRef]
14. Gohar, R. Oil Film Thickness and Rolling Friction in Elastohydrodynamic Point Contact. *J. Lubr. Technol.* **1971**, *93*, 371–379. [CrossRef]
15. Bahadoran, H.; Gohar, R. The oil film in elastohydrodynamic elliptical contacts. *Wear* **1974**, *29*, 264–270. [CrossRef]
16. Bronstein, I.N.; Semendjajew, K.A. *Taschenbuch der Mathematik*, 11th ed.; Europa-Lehrmittel: Haan, Germany, 2020.
17. Grekoussis, T.R.; Michailidis, M.R. Näherungsgleichung zur Nach- und Entwurfsrechnung der Punktberührung nach Hertz. *Konstruktion* **1988**, *33*, 135–139.
18. Deulin, E.A.; Mikhailov, V.P.; Panfilov, Y.V.; Nevshupa, R.A. *Mechanics and Physics of Precise Vacuum Mechanisms*; Fluid Mechanics and Its Applications; Springer: Dordrecht, The Netherlands, 2012.
19. Brecher, C.; Rossaint, J.; Hassis, A. Cage Friction in High-Speed Spindle Bearings. *Tribol. Trans.-Off. J. Soc. Tribol. Lubr. Eng.* **2014**, *57*, 77–85. [CrossRef]
20. Hong, S.W.; Tong, V.C. Rolling-element bearing modeling: A review. *Int. J. Precis. Eng. Manuf.* **2016**, *17*, 1729–1749. [CrossRef]
21. Tüllmann, U. Das Verhalten Axial Verspannter, Schnelldrehender Schrägkugellager. Ph.D. Thesis, RWTH Aachen, Aachen, Germany, 1999.
22. Gupta, P.K. Minimum Energy Hypothesis in Quasi-Static Equilibrium Solutions for Angular Contact Ball Bearings. *Tribol. Trans.* **2020**, *63*, 1051–1066. [CrossRef]
23. Falker, J. Analyse des Betriebsverhaltens von Hochgeschwindigkeits-Wälzlagern unter Radialen Lasten. Ph.D. Thesis, RWTH Aachen, Aachen, Germany, 2019.
24. SKF. *Super-Precision Bearings*; SKF: Gothenburg, Sweden, 2014.
25. Klüber. *Klübersynth FB 4-32, 4-46, 4-68*. Munich, 2021. Available online: https://www.klueber.com/de/de/downloads (accessed on 12 March 2023).
26. Klüber. *Klüberspeed BF 72-22*. Munich, 2020. Available online: https://www.klueber.com/de/de/downloads (accessed on 15 March 2023).
27. Gärtner, M.; Brecher, C.; Neus, S.; Eckel, H.M.; Bartelt, A.; Hoppert, M.; Ilkhani, M.R. The Friction of Radially Loaded Hybrid Spindle Bearings under High Speeds. 2023. Available online: https://zenodo.org/record/7986707 (accessed on 1 March 2023).
28. Brecher, C.; Bartelt, A.; Fey, M.; Hassis, A.; Lehner, B. Einflussfaktoren auf das Reibmoment Öl-Luft-geschmierter Spindellager. *Tribol. Schmier.* **2018**, *65*, 26–30.
29. Brecher, C.; Weck, M. (Eds.) *Machine Tools Production Systems 2: Design, Calculation and Metrological Assessment*; Springer: Berlin/Heidelberg, Germany, 2021; Volume 2. [CrossRef]
30. Brecher, C.; Fey, M.; Falker, J. Simulation schnelldrehender Wellen-Lager-Systeme -Teil 1: Berechnung von Hochgeschwindigkeitswälzlagern in Wellen-Lager-Systemen. *Antriebstechnik* **2019**, *58*, 66–72.
31. Schulz, A.; Körner, G. NewSpilad Version 1.0c—Berechnungsprogramm des Werkzeugmaschinenlabors der RWTH Aachen. Technical Report. 2002. Available online: https://books.google.de/books?id=kmMhBAAAQBAJ&pg=PA687&lpg=PA687&dq=NewSpilad+Version+1.0c---Berechnungsprogramm+des++Werkzeugmaschinenlabors&source=bl&ots=kYYCgm3_Hh&sig=ACfU3U0vVznsunYGTSQYoL4piob50g2cVw&hl=en&sa=X&ved=2ahUKEwiC6cj3pcP_AhURxwIHHUn6CV0Q6AF6BAgIEAM#v=onepage&q=NewSpilad (accessed on 20 March 2023).

32. Butz, F.; Tüllmann, U. WinLager2v0—Berechnungsprogramm des Werkzeugmaschinenlabors der RWTH Aachen. Technical Report. 2003. Available online: https://books.google.de/books?id=kmMhBAAAQBAJ&pg=PA687&lpg=PA687&dq=NewSpilad+Version+1.0c---Berechnungsprogramm+des++Werkzeugmaschinenlabors&source=bl&ots=kYYCgm3_Hh&sig=ACfU3U0vVznsunYGTSQYoL4piob50g2cVw&hl=en&sa=X&ved=2ahUKEwiC6cj3pcP_AhURxwIHHUn6CV0Q6AF6BAgIEAM#v=onepage&q=NewSpilad (accessed on 20 March 2023).

33. Wang, L.; Wood, R.; Harvey, T.; Morris, S.; Powrie, H.; Care, I. Wear performance of oil lubricated silicon nitride sliding against various bearing steels. *Wear* **2003**, *255*, 657–668. [CrossRef]